Multiple Gaussian process models based global sensitivity analysis and efficient optimization of in vitro mRNA transcription process

Min Tao[a], Adithya Nair[a], Ioanna Kalospyrou[a], Robert A Milton[a], Mabrouka Maamra[a], Zoltan Kis[a], Joan Cordiner[a], Solomon F Brown[a]

[a]*School of Chemical, Materials and Biological Engineering , The University of Sheffield, S10 2TN, UK*

Abstract

The in vitro transcription (IVT) process is a critical step in RNA production. To ensure the efficiency of RNA manufacturing, it is essential to optimize and identify its key influencing factors. In this study, multiple Gaussian Process (GP) models are used to perform efficient optimization and global sensitivity analysis (GSA). Firstly, multiple GP models were constructed using the data from multiple experimental replicates, accurately capturing the complexities of the IVT process. Then GSA was conducted to determine the dominant reaction factors, specifically the concentrations of reactants NTP and Mg across all data-driven models. Concurrently, a multi-start optimization algorithm was applied to these GP models to identify optimal operational conditions that maximize RNA yields across all surrogate models. These optimized conditions are subsequently validated through additional experimental data.

Keywords: In vitro mRNA transcription, Multiple Gaussian process models, Global sensitivity analysis, Efficient optimization, Data-driven models

1. Introduction

Vaccines have been an effective strategy for combating epidemics and pandemics over the past decades [1]. The rapid outbreak and spread of the recent coronavirus disease 2019 (COVID-19) posed significant challenges for pandemic response, but also provided a crucial opportunity for the development

and breakthrough of the novel messenger RNA (mRNA) vaccine platform technology [2]. Since the potential of this innovative vaccine platform technology was realized, efforts have been directed towards its utilization in both preventive and therapeutic applications [3] . Notably, recent technological advancements have enabled this platform to facilitate the rapid development of vaccine candidates against multiple infectious diseases and several types of cancers [4].

Compared to traditional vaccine platforms, mRNA technology offers significant advantages. Specifically, mRNA is highly precise, safer and more efficient in eliciting the desired immune response [5]. Additionally, mRNA production occurs through an *in vitro* cell-free transcription reaction [6], eliminating concerns about cell-derived impurities and viral contaminants, which are common safety concerns in traditional vaccines[7]. mRNA technology also surpasses DNA vaccine platforms. Unlike DNA, mRNA expression does not require entry into the nucleus, thus avoiding risks such as the generation of infectious particles or random integration in the host cell genome [8]. From a manufacturing standpoint, mRNA technology is particularly beneficial as changes in the encoded antigen do not alter the physicochemical properties of the mRNA backbone [9]. This allows for a standardized production process, which could revolutionize therapeutic vaccine manufacturing and significantly impact the treatment of chronic diseases. Nevertheless, there is considerable scope for improving the RNA manufacturing process , particularly in increasing production rates and reducing costs. The slow pace of vaccine manufacturing [10] was a major obstacle to rapid deployment of RNA vaccines during the recent pandemic [11]. To ensure efficient, high-quality RNA manufacturing and swift responses to future pandemics, the integration of digital tools into production processes will be critical for driving substantial improvements [12].

The complex manufacturing processes for mRNA vaccines typically involve two main stages: drug substance manufacturing and product manufacturing. Drug substance manufacturing begins with upstream IVT processing, followed by purification through filtration and chromatography. Product manufacturing, on the other hand, focuses on encapsulating RNA into lipid nanoparticles (or other delivery systems), followed by further purification (commonly using tangential flow filtration and sterile filtration). Finally the fill-finish or secondary manufacturing stage involves filling the drug substance into glass vials or other container [7]. To efficiently optimize operating conditions and identify the key reagents in the upstream IVT reaction process

(and other unit operations), model based computational tools such as optimization and global sensitivity analysis are essential. These tools can be constructed using mechanistic and/or data-driven process models. Therefore, the development of these computational tools fundamentally depends on effective model development.

Over the years, several mathematical models have been developed to quantify the products of the IVT batch bioreactor based on an evolving understanding of the IVT reaction mechanism. Initially, kinetic models with rate expressions were constructed to describe the RNA polymerization process, accounting for the influence of DNA template concentration [13]. Subsequently, a multi-physical IVT model was introduced, capturing the coupled phenomena of the transcription reaction and precipitation formation [14]. Following this, combined models incorporating both multi-physical and empirical approaches were developed to account for a broader range of operating conditions, with experimental data used for parameter estimation [12]. These models were later applied to conduct global sensitivity analysis, identifying key factors influencing RNA yield. More recently, a detailed mechanistic model was created to describe the nucleation and growth of precipitation phenomena, incorporating the effect of sequence length on transcription rate [15]. However, given that the full complexity of reaction mechanism has not yer been fully characterized in a comprehensive mathematical form, it may be impractical to rely solely on the current IVT mechanistic model for global sensitivity analysis and optimization.

In parallel, data-driven computational methodologies have been rapidly evolved, driven by the success of machine learning techniques. Common data-driven approaches include simple polynomial models, neural network models and Gaussian process models [16]. While simple polynomial functions are often too basic to capture complex manufacturing processes. Early research of IVT models focuses on constructing empirical models using experiment data for short-length RNA transcription process [17], which is not suitable for more practical manufacturing process on producing longer RNA molecules. While neural network (NN) models can predict the arbitrary complex systems with mathematical guarantees [18]. However, building NN models requires huge number of samples, leading to expensive costs of experiment time and materials for the IVT process, which is inefficient and unrealistic. Gaussian process (GP) models are the probabilistic machine learning approach, which assumes that the outcome function values as random variables and can predict the uncertainty of outcome values with less samples. Recently, a GP

based Bayesian optimisation strategy has been proposed to maximize the RNA yield within the limited number of experiments [19]. However, it has not considered the multiple local optimums of the iterative complex nonlinear optimization problem, which may lead to undesirable iterative solutions and consume more experiments. In addition to single physical and data-driven approaches, hybrid models combining mechanistic and data-driven methods, may offer an alternative solution. [20]. Nevertheless, the question of how to efficiently construct hybrid models for such complex IVT reaction systems remains unresolved.

In this work, we leverage the powerful probabilistic GP models to construct efficient global sensitivity analysis and optimization frameworks for IVT processes. The primary novelty lies in the proposed multiple GP models based the computational methodologies of efficient global sensitivity analysis and optimization for complex stochastic IVT systems. Specifically, multiple GP models are firstly constructed based on the different replicates of experiments and their average. Then a global sensitivity analysis framework is applied on these GP models to identify the dominant factors consistently across all models. In parallel, an efficient multi-start optimization strategy was performed on these GP models to identify operational conditions yielding high RNA production across all constructed GP models. To the best of our knowledge, this is the first study in the literature to employ multiple GP models based computational frameworks for practical stochastic bio-processes. This approach offers a robust method for analyzing variability and optimizing in biotechnological processes, particularly within the context of IVT systems.

The remainder of this paper is structured as follows: Section 2 provides a brief overview of the IVT reaction process and the experimental procedures employed. Section 3 introduces the Gaussian process model focusing on multiple GP models relevant to IVT systems. Section 4 details the multi-GP based global sensitivity analysis framework developed for IVT processes , while Section 5 presents our proposed multi-GP based optimization strategy for these processes. Finally, Section 6 concludes the paper, discussing our findings and exploring potential further applications of these methodologies.

2. IVT reaction process and experimental sampling design

2.1. Process description

In vitro transcription (IVT) reaction is the process of encoding a specific region of a DNA template into mRNA. For mass production of mRNA, transcription occurs *in vitro* , in a cell-free environment within a bioreactor. The reaction is catalyzed by enzymes called RNA polymerases and takes place in a buffer solution with magnesium being its most crucial component. Figure 1 illustrates the general mechanism of the IVT reaction [17, 21]. In Step 2 of the figure, nucleoside triphosphates (NTPs) are mentioned. These consist of a sugar molecule, a nitrogenous base, and three phosphate groups. In contrast, nucleoside monophosphates (NMPs), which form the building blocks of the RNA chain, contain only a single phosphate group.

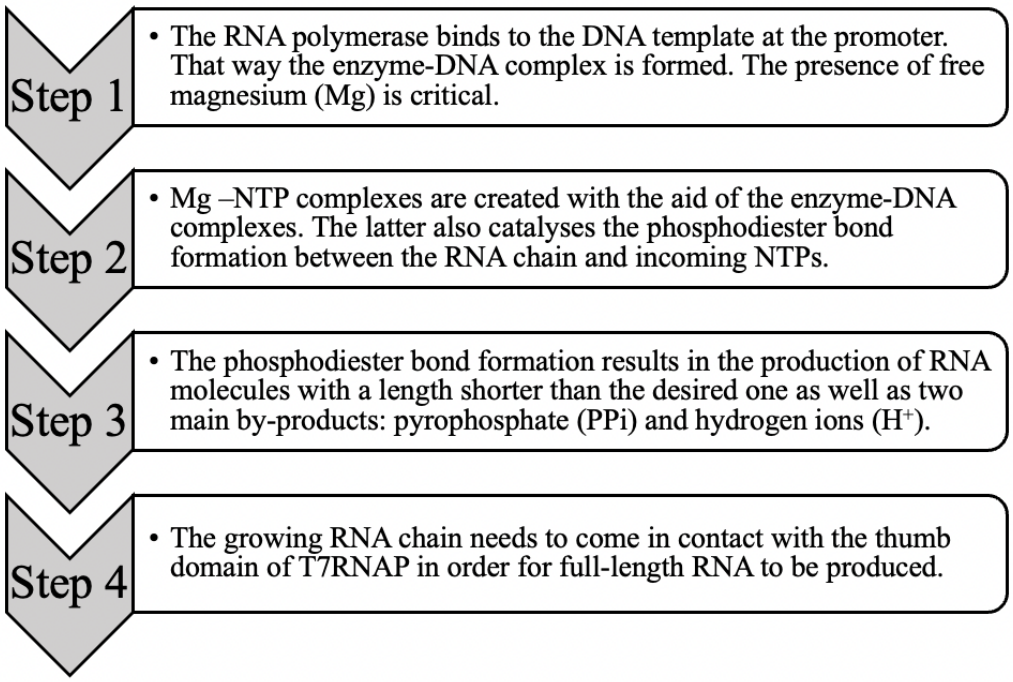

Figure 1: *In vitro* transcription mechanism.

In this study, SARS-CoV-2 Spike protein mRNA transcripts were prepared using an in-vitro transcription (IVT) reaction. The reaction utilized template DNA (linearized plasmid containing SARS-CoV-2 Spike protein gene and T7 polymerase promoter sequence). DNA-dependent RNA

polymerase from T7 bacteriophage (Roche, Germany) and ribonucleotides (Roche, Germany) ATP, CTP, GTP and UTP were added to the reaction mixture. The reaction was further supplemented with Magnesium Acetate (enzyme cofactor), HEPES buffer (buffering agent), Dithiothreitol (reducing agent to prevent enzyme oxidation), Sodium Chloride and Spermidine. Inorganic pyrophosphatase (Roche, Germany) was added to prevent Magnesium pyrophosphate precipitation. RNase inhibitor (Roche, Germany) was included to maintain an RNase-free environment in the reaction mixture. The IVT reaction mixture volume was fixed at 100 uL with a PH of 7.0. The reaction mixture was incubated at 37 °C . After incubation, the reaction was quenched by adding EDTA (sequestering Mg2+ ions). For RNA concentration measurement by UV absorbance, the mRNA was purified from the IVT reaction mixture using a Monarch RNA Cleanup Column (NEB) according to the manufacturer's recommended protocol. Purified mRNA was quantified using a NanoDrop Spectrophotometer (Thermo Scientific) by measuring absorbance at 260 nm.

2.2. Experimental sampling design

To optimize the operational conditions and identify the dominant factors affecting mRNA yield of the aforementioned reaction process, we focused on six important factors based on our prior knowledge, including concentrations of DNA template, the substrate as NTPs, the enzyme as T7 polymerase, spermindine, Mg+ concentration and incubation time. Then a systematic Design of Experiment (DoE) was implemented to obtain efficient datasets for model construction. The ranges of these six design parameters are presented in Table 1 as below.

Table 1: Ranges of design parameters for IVT reaction

Name	Units	Range
DNA template	ug/ml	[100, 400]
NTPs	mM	[4, 60]
T7 polymerase enzyme	Unit/ul	[100, 400]
Spermidine	mM	[0.5, 4]
Mg+ concentration	mM	[6, 90]
Incubation time	h	[0.25, 4]

There are several popular DoE sampling techniques such as full factorial design [22] and Latin Hypercube (LHC) [23] that can produce high-quality

results. The full factorial design is a comprehensive approach that considers all possible combinations of discrete values (levels) across factors but does not introduce randomness into the experimental design. In contrast, the LHS method ensures broader coverage of the design space by maximizing the diversity among the generated samples. It divides the sample domain into multiple sub-domains, where random sample points are generated to accurately represent each sub-domain. This enables a more efficient exploration of the entire parameter space.

In this work, we selected Latin Hypercube Sampling (LHS) for our DoE approach due to its proven ability to effectively explore the design space and better capture input-output relationships. For determining the number of LHS samples, a small initial sample size combined with sequential adaptive sampling via Bayesian optimization can be one potential approach [24]. However, this method may fail to cover certain important regions of the parameter space due to inaccurate initial surrogate models or inefficient optimization processes. To address this, we employed a relatively large number of initial experimental samples to build accurate surrogate models for the complex IVT systems across the whole range. These models were then used for optimization to identify operating conditions that yield high RNA production. In this study, we generated 60 LHC samples for the DoE, with each sample replicated twice experimentally. This resulted in two sets of 60 experiments, each with six inputs (factors) and one output (mRNA yield). Then the average mRNA yield across the two replicates was calculated, creating an additional output. Thus, three input-output datasets were obtained: the two original replicates and one averaged dataset, all using the sample LHC inputs but yielding different mRNA outputs. Figure 2 illustrates the three input-output data sets, showing that the 60 LHC samples broadly cover the parametric space defined by the six key design factors.

The mRNA yields varied significantly across the datasets, reflecting possible experimental errors and the inherent stochasticity of the complex IVT process. Specifically, for approximately 18% of the experimental conditions, the yield difference between the two replicates exceeded 4 g/L, and for around 13 %, the difference was greater than 6 g/L. This substantial uncertainty in the original data highlights the need for multiple GP surrogate models to capture more information from the different replicates. It is important to note that while 60 samples with two replicates may not be sufficient to fully capture the complex behavior of IVT systems, this limitation is common in early-stage biological process development due to the high costs associated

with experimentation.

In the following sections, multiple GP surrogates will be constructed to represent the complex system dynamic more effectively. These surrogates will be utilized to identify the key factors influencing mRNA yield and to optimally determine the operating conditions that yield high mRNA production.

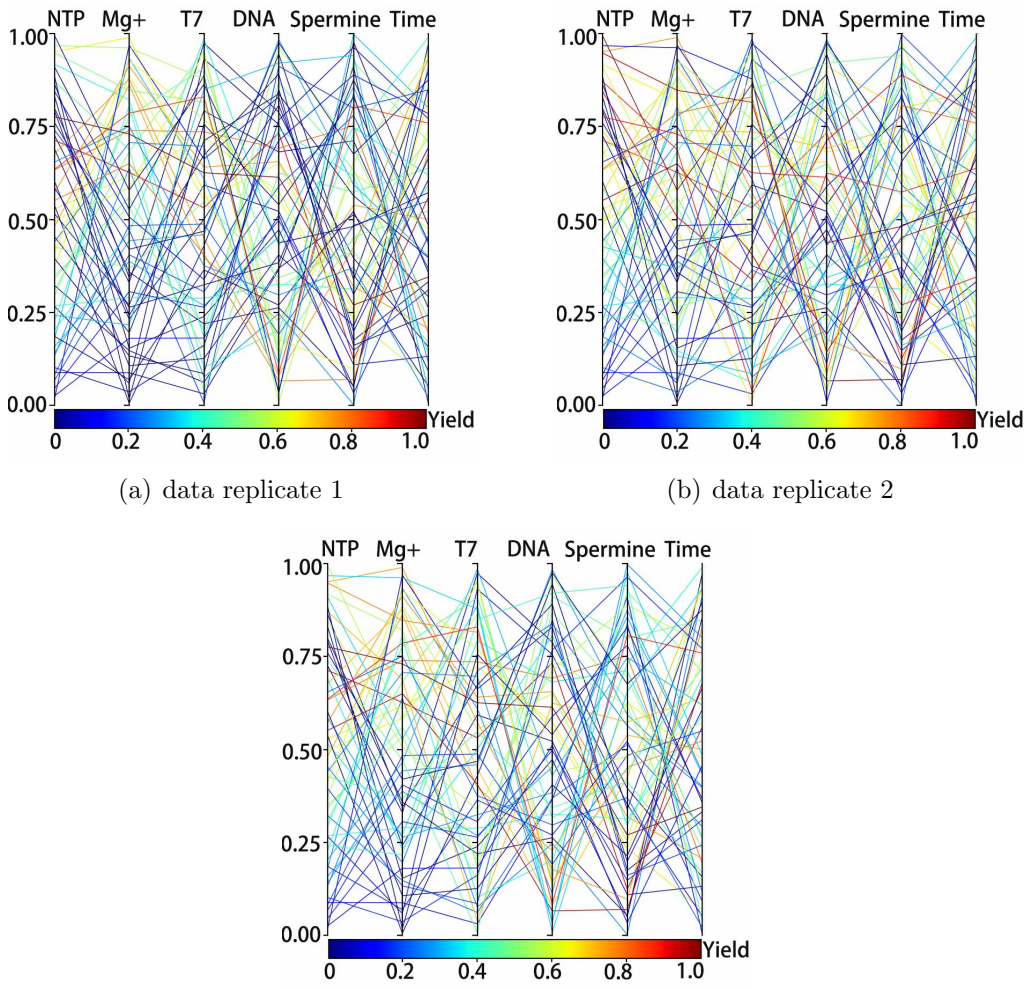

(a) data replicate 1

(b) data replicate 2

(c) the average data of two replicates

Figure 2: Normalized parametric space coverage of 60 LHC samples with corresponding mRNA yield (indicated by the colour bar)

3. Multiple Gaussian process models for IVT processes

In this section, we present the Gaussian process (GP) models used in this study, as well as the proposed multiple GP models tailored for the IVT process. These models will be further applied within optimization and global sensitivity analysis frameworks to enhance understanding and improve process performance.

3.1. Gaussian process model

In this work, we employed GP surrogate models to establish an explicit relationship between the IVT reagent components, denoted as $\boldsymbol{x}$ and the mRNA yield $\boldsymbol{y} = \boldsymbol{f}(\boldsymbol{x}) + \boldsymbol{\sigma}_e^2 \boldsymbol{I_f}$, where $\boldsymbol{\sigma}_e^2$ represents the observed data noises and $\boldsymbol{I_f}$ is the identity matrix. GP regression is a powerful non-parametric modeling techniquewidely utilized in probabilistic machine learning applications [25]. A key assumption of GP regression is that the random output variables $\boldsymbol{f}(\boldsymbol{x_i})$ at any input point $\boldsymbol{x_i}$ follows a normal distribution with a mean value $\boldsymbol{\mu}(\boldsymbol{x_i})$ and variance $\boldsymbol{\sigma^2}(\boldsymbol{x_i})$. The prior joint Gaussian distribution $\boldsymbol{f}(\boldsymbol{X})$ for a set of finite random variables $\boldsymbol{X} = (\boldsymbol{x_1}, \boldsymbol{x_2} ... \boldsymbol{x_n})$ is given as:

$$\begin{aligned} \boldsymbol{f}(\boldsymbol{X}) &\sim \boldsymbol{N}(\boldsymbol{\mu}(\boldsymbol{X}), \boldsymbol{\sigma^2}(\boldsymbol{X})) \\ \boldsymbol{y}|\, \boldsymbol{f} &\sim \boldsymbol{N}(\boldsymbol{f}, \boldsymbol{\sigma}_e^2 \boldsymbol{I}_f) \end{aligned} \tag{1}$$

Here, $\boldsymbol{f}(\boldsymbol{X}) = (\boldsymbol{f}(\boldsymbol{x_1}), \boldsymbol{f}(\boldsymbol{x_2}) ... \boldsymbol{f}(\boldsymbol{x_n}))$, $\boldsymbol{\mu}(\boldsymbol{X}) = (\boldsymbol{\mu}(\boldsymbol{x_1}), \boldsymbol{\mu}(\boldsymbol{x_2}) ... \boldsymbol{\mu}(\boldsymbol{x_n}))$, $\boldsymbol{\sigma^2}(\boldsymbol{X}) = (\boldsymbol{\sigma^2}(\boldsymbol{x_1}), \boldsymbol{\sigma^2}(\boldsymbol{x_2}) ... \boldsymbol{\sigma^2}(\boldsymbol{x_n}))$ where $\boldsymbol{n}$ represents the number of samples, The mean function is typically set to zero, and the covariance matrix $\boldsymbol{\sigma^2}(\boldsymbol{X})$ is expressed as the kernel matrix $\boldsymbol{K}(\boldsymbol{X}, \boldsymbol{X})$ with each element $\boldsymbol{K}_{i,j} = \boldsymbol{k}(\boldsymbol{x_i}, \boldsymbol{x_j})$.

In this work, a common radial basis function kernel was used for the GP models as it is known for its efficiency in handling complex, real-world cases through automatic relevance determination (ARD) kernels [26]. This kernel also allows for semi-analytical computations, making it useful for further applications such as optimization and sensitivity analysis [27]. The GP kernel function formulation assumes that when two inputs points $\boldsymbol{x_j}, \boldsymbol{x_i}$ are close in the input space, their corresponding outputs $\boldsymbol{f}(\boldsymbol{x_j})$ and $\boldsymbol{f}(\boldsymbol{x_i})$ are also close. The kernel function is formulated as:

$$\boldsymbol{k}(\boldsymbol{x_i}, \boldsymbol{x_j}) = \boldsymbol{\sigma_f^2} \boldsymbol{exp}(-\frac{\boldsymbol{1}}{\boldsymbol{2l^2}} (\boldsymbol{x_i} - \boldsymbol{x_j})^{\boldsymbol{T}} (\boldsymbol{x_i} - \boldsymbol{x_j})) \tag{2}$$

Here, $\boldsymbol{\sigma_f^2}$ is a global scale parameter and $\boldsymbol{l} = (\boldsymbol{l_1, l_2 ... l_d})$ represents the bandwidth parameters where $\boldsymbol{d}$ is the dimensionality of the inputs.

Given prior samples $\boldsymbol{(X, Y)}$, the predictive function value $\boldsymbol{f(X')}$ at a new location $\boldsymbol{X'}$ and the prior function outputs $\boldsymbol{f(X)}$ follow a joint Gaussian distribution:

$$\begin{bmatrix} \mathbf{f}(\mathbf{X}') \\ \mathbf{f}(\mathbf{X}) \end{bmatrix} \sim N(\begin{bmatrix} \mathbf{0} \\ \mathbf{0} \end{bmatrix}, \begin{bmatrix} \mathbf{K}(\mathbf{X}', \mathbf{X}') & \mathbf{K}(\mathbf{X}', \mathbf{X}) \\ \mathbf{K}(\mathbf{X}, \mathbf{X}') & \mathbf{K}(\mathbf{X}, \mathbf{X}) + \sigma_{\mathbf{e}}^{\mathbf{2}}\mathbf{I}_{\mathbf{f}} \end{bmatrix}) \tag{3}$$

The posterior predictive distribution $\boldsymbol{y(X')|\,(X, Y)}$, given the data noise $\boldsymbol{\sigma}_e^2$, can be computed as:

$$\begin{aligned} \boldsymbol{y(X')|\,(X, Y) \sim N(K(X', X)(K(X, X) + \sigma_e^2 I_f)^{-1} Y,} \\ \boldsymbol{K(X', X') - K(X', X')(K(X, X) + \sigma_e^2 I_f)^{-1} K(X, X') + \sigma_e^2 I_f)^{-1} Y)} \end{aligned} \tag{4}$$

The hyper-parameters $\boldsymbol{\sigma_f}$, $\boldsymbol{l}$ and $\boldsymbol{\sigma}_e$ are obtained through maximizing the log marginal likelihood $\rho(\boldsymbol{y|\,\sigma_f, l, \sigma_e})$ on the collected data $\boldsymbol{(X, Y)}$, given by:

$$\log\ \rho(\boldsymbol{y|\,\sigma_f, l, \sigma_e}) = -\frac{\boldsymbol{n}}{2} \log\ 2\pi - \frac{1}{2} \log |K(\boldsymbol{X, X}) + \boldsymbol{\sigma_e^2 I_f}| - \frac{1}{2} \boldsymbol{Y}^T (K(\boldsymbol{X, X}) + \boldsymbol{\sigma_e^2 I_f})^{-1} \boldsymbol{Y} \tag{5}$$

All GP models in this study were implemented using our open-source ROM-COMMA software library [28] .

3.2. Multiple GP models for IVT processes

As described in Section 2.2 of the Design of Experiment, two replicates of experimental data were collected, and the average of these replicates was computed to generate an additional output dataset. This averaged dataset, along with the input LHC samples, formed a separate dataset. Together, these three datasets were used to build three distinct GP models for the IVT processes. These models will be instrumental in constructing the frameworks for efficient optimization and global sensitivity analysis. The general approach for constructing multiple GP models is outlined in Algorithm 1.

Algorithm 1 Multiple GP model construction algorithm for IVT processes

Inputs: $\boldsymbol{\Omega}$: design space range; N: number of Latin hypercube samples (N =60); $\boldsymbol{X}$: generated N Latin hypercube samples ; $\boldsymbol{Y_1}$: experiment data for replicate 1 under conditions $\boldsymbol{X}$; $\boldsymbol{Y_2}$: experiment data for replicate 2 under conditions $\boldsymbol{X}$.

Outputs: Hyper-parameters for GP1 model (replicate 1) : $\boldsymbol{\sigma_{f1}, l^1, \sigma_{e1}}$ Hyper-parameters for GP2 model (replicate 2) : $\boldsymbol{\sigma_{f2}, l^2, \sigma_{e2}}$ Hyper-parameters for GP3 model (average data): $\boldsymbol{\sigma_{f3}, l^3, \sigma_{e3}}$

1: **Generate** N Latin hypercube samples in the design space $\boldsymbol{\Omega}$

2: **Collect** experiment data for replicates $\boldsymbol{Y_1}$ and $\boldsymbol{Y_2}$ under $\boldsymbol{X}$, compute average $\boldsymbol{Y_3 = (Y_1 + Y_2)/2}$

3: **Compute** the hyper-parameters $\boldsymbol{\sigma_{f1}, l^1, \sigma_{e1}}$ for GP1 through maximizing the marginal likelihood Eq.(5), and obtain the posterior predictive distribution $\boldsymbol{y_1(X')|\,(X, Y_1)}$ as Eq.(4)

4: **Compute** the hyper-parameters $\boldsymbol{\sigma_{f2}, l^2, \sigma_{e2}}$ for GP2 and obtain the posterior predictive distribution $\boldsymbol{y_2(X')|\,(X, Y_2)}$ as Eq.(4)

5: **Compute** the hyper-parameters $\boldsymbol{\sigma_{f3}, l^3, \sigma_{e3}}$ for GP3 model and obtain the posterior predictive distribution $\boldsymbol{y_3(X')|\,(X, Y_3)}$ as Eq.(4)

6: **return** Hyper-parameters for all three GP models

The above Algorithm 1 was applied to three data sets, resulting in three distinct GP models: GP1, derived from data replicate 1; GP2, from data replicate 2; and GP3, from the averaged data. Specifically, we employed our open-source software ROM-COMMA to generate these GP models using a 10-fold cross-validation method after pre-processing the inputs and outputs.

Table 1 presents the evaluation of all three model evaluations based on three metrics: Root Mean Square Error (RMSE), R-squared (R^2) and the proportion of outliers. The models demonstrated strong performance, as indicated by relatively low RMSE values (less than 0.4) , high R^2 values (greater than 0.87), and a low proportion of outliers (0.0167). These results suggest that the training processes and predictions of all three GP models were robust and accurate. Additionally, Figures 3 and 4 below illustrate the comparison between the original data and the GP model predictions. The differences between the experimental data and the mean predictions from the GP models were minimal, further indicating efficient model training. Moreover, the GP models provide uncertainty quantification through the confidence intervals of the predictive posterior distributions at the 95% confidence level. Notably,

the confidence intervals were relatively narrow at most predictive locations except for GP1, where the intervals were larger compared to GP2 and GP3. This discrepancy in GP1 could be attributed to higher noise levels in data replicate 1.

It is important to note that, due to the limited dataset size (60 samples), the generated GP models may not fully capture all system's behaviours. However, utilizing all three GP models for optimization and global sensitivity analysis aims to enhance the accuracy of the predictions as much as possible.

Table 2: Detailed information for GP model evaluations

Model	RMSE	R^2	Outliers
GP1	0.359	0.871	0.0167
GP2	0.357	0.872	0.0167
GP3	0.344	0.881	0.0167

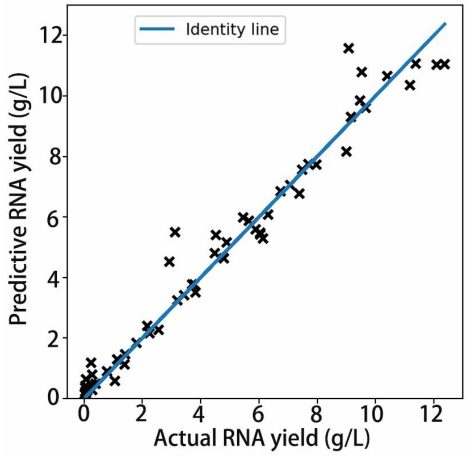

(a) data replicate 1

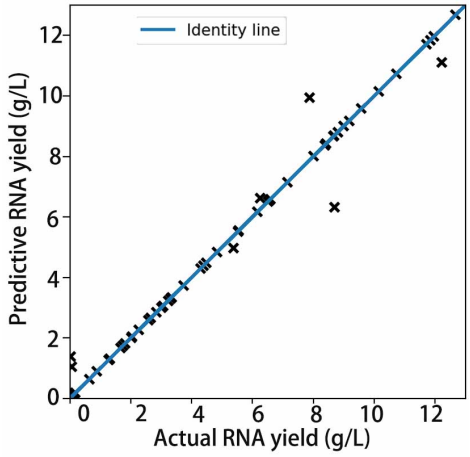

(b) data replicate 2

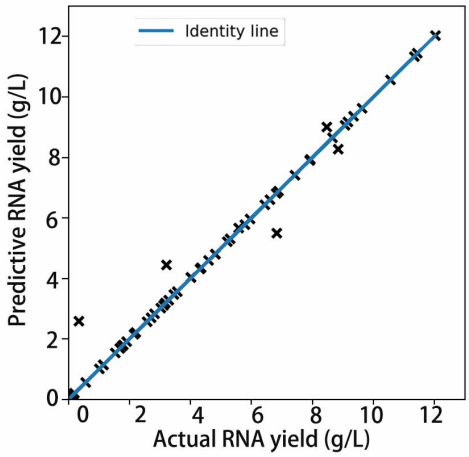

(c) the averaged data

Figure 3: Comparisons between the mean mRNA yield prediction and experimental data: (a) GP1 model based on data replicate 1 (b) GP2 model based on data replicate 2 (c) GP3 model base on the averaged data

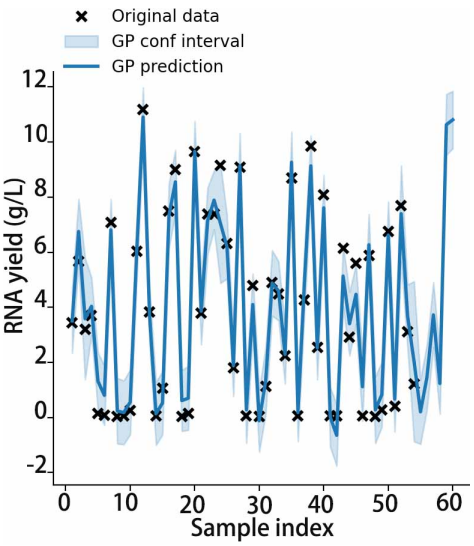

(a) data replicate 1

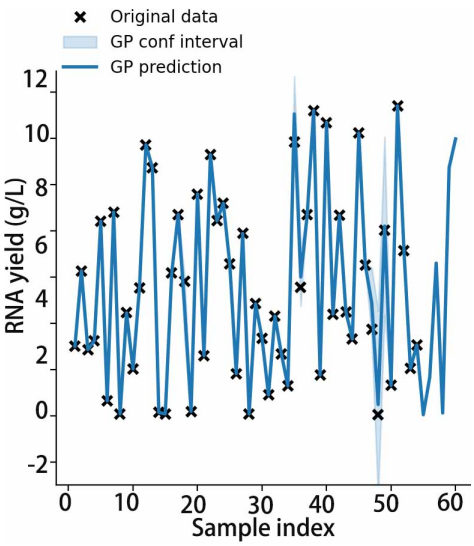

(b) data replicate 2

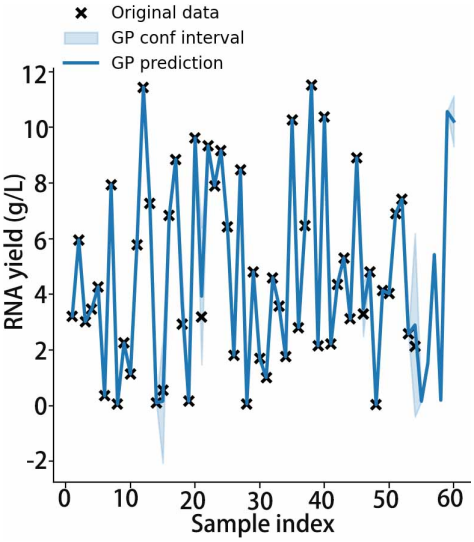

(c) the average data of two replicates

Figure 4: Comparison between the mRNA yield prediction and experimental data: (a) GP1 model based on data replicate 1 (b) GP2 model based on data replicate 2 (c) GP3 model based on the averaged data

4. Multiple GP models based global sensitivity analysis for IVT processes

Global sensitivity analysis (GSA) quantifies how uncertainty in model outputs can be attributed to the uncertainty in individual inputs or their combinations [29, 30]. It is a powerful tool for identifying key input variables that drive system outputs. In this section, we introduce GSA, combined with the proposed multiple Gaussian process (GP) models, to identify the dominant factors influencing mRNA yield in complex IVT processes.

4.1. Variance-based Global sensitivity analysis

The variance-based GSA method, commonly referred to as the Sobol' indices, measures the proportion of output variance attributed to each individual input or combination of inputs [29]. The GP surrogate model with automatic relevance determination (ARD) kernels facilitates semi-analytic calculations, further accelerating computational speed. Specifically, the variance-based GSA is performed on the mean predictive function:

$$\boldsymbol{\mu_*(X')} = \boldsymbol{K(X', X)(K(X, X) + \sigma_e^2 I_f)^{-1} Y} \tag{6}$$

From a probabilistic perspective, the inputs and outputs, represented by $\boldsymbol{(X', \mu_*(X'))}$, are considered random variables. The key idea behind the Sobol' indices method is to decompose the variance of the random outputs $\mu_*(\boldsymbol{X'})$:

$$\boldsymbol{Var(\mu_*)} = \sum_{\boldsymbol{i=1}}^{\boldsymbol{d}} \boldsymbol{V_i} + \sum_{\boldsymbol{i<j}}^{\boldsymbol{d}} \boldsymbol{V_{ij}} + \boldsymbol{...} + \boldsymbol{V_{12...d}} \tag{7}$$

where $\boldsymbol{V_i = Var_{X_i'}(E(Y|X_i'), V_{i,j} = Var_{X_{i,j}'}(E(Y|(X_i', X_j')) - V_i - V_j}$ and so on.

The first-order Sobol' index $\boldsymbol{S_i}$, quantifying the effect of a single input $\boldsymbol{X_i'}$, is computed as:

$$\boldsymbol{S_i} = \frac{\boldsymbol{V_i}}{\boldsymbol{Var(\mu_*)}} \tag{8}$$

Next, the cumulative first-order index $\boldsymbol{S^j}$, quantifying the combined effects of the inputs ($\boldsymbol{X_1', X_2', X_3', ..., X_j'}$ on the total variance, can be calculated as :

$$\boldsymbol{S^j} = \sum_{\boldsymbol{i=1}}^{\boldsymbol{j}} \boldsymbol{S_i} \tag{9}$$

where $\boldsymbol{j(j = 1, 2, ..., d)}$ represents the position in the input index order $\boldsymbol{\alpha = \{1, 2, ..., d\}}$.

We also compute the closed Sobol' index $\boldsymbol{S^C_{\psi_j}}$, representing the combined effects of the inputs $\boldsymbol{X'_1, X'_2, X'_3, ..., X'_j}$, as follows:

$$\boldsymbol{S^C_{\psi_j} = \sum_{\psi_i} S_{\psi_i}, \psi_i \subseteq \psi_j \& \psi_i \neq \varnothing} \tag{10}$$

where $\boldsymbol{\psi_j = \{1, 2, ..., j\} \subseteq \alpha}$ is the index set of inputs $\boldsymbol{X'_1, X'_2, X'_3, ..., X'_j}$.

The interaction effects $\boldsymbol{S_{\sim_j}}$ among the first inputs $\boldsymbol{X'_1, X'_2, X'_3, ..., X'_j}$ are then calculated as:

$$\boldsymbol{S_{\sim_j} = S^C_{\psi_j} - S^j} \tag{11}$$

In this work, we focus on identifying key input parameters by comparing the cumulative first-order indices $\boldsymbol{S^j}$ and the closed indices $\boldsymbol{S^C_{\psi_j}}$ within the order $\boldsymbol{\alpha}$, arranged by decreasing first-order index in GSA test computations. This approach helps to identify the most important input group.

4.2. Multiple GP models based global sensitivity analysis

Building on the three GP models, we propose a multiple GP models based global sensitivity analysis framework to identify the key factors in the IVT process. Unlike the standard one GP based GSA approach discussed in Section 4.1, this multiple GP model based GSA leverages all three GP models of the complex IVT process to improve the likelihood of identifying the most influential inputs. This approach may provide valuable insights for reducing material usage and optimizing the process further.

The additional computational steps involve performing the GSA calculations, as outlined in Eq.(7-10), to compute the first-order indices $\boldsymbol{S_i}$ for each input factor and the corresponding closed indices $\boldsymbol{S^C_{\psi_i}}$. Based on the computed first-order and closed-order indices, the key inputs across all three GP models can be determined. The detailed procedures for the multiple GP models based global sensitivity analysis of IVT processes are described below.

Algorithm 2 Multi- GP based global sensitivity analysis for IVT processes

Inputs: $(\boldsymbol{X}, \boldsymbol{Y_1})$: data set from experiment replicate 1; $(\boldsymbol{X}, \boldsymbol{Y_2})$: data set from experiment replicate 2; $(\boldsymbol{X}, \boldsymbol{Y_3})$: data set of the averaged data; GP1 model (data replicate 1) $\boldsymbol{y_1(X')}|\,(\boldsymbol{X}, \boldsymbol{Y_1})$; GP2 model (data replicate 2) $\boldsymbol{y_2(X')}|\,(\boldsymbol{X}, \boldsymbol{Y_2})$; GP3 model (averaged data) $\boldsymbol{y_3(X')}|\,(\boldsymbol{X}, \boldsymbol{Y_3})$

Outputs: $\boldsymbol{\psi^*}$: the important input group across all three GP models

1: **Compute** the first-order index $\boldsymbol{S1_i}$ and closed-order index $\boldsymbol{S1^C_{\psi_i}}$, through performing the GSA computations as Eq.(7-10) on the mean prediction $\mu_{1*}(\boldsymbol{X'}) = \boldsymbol{K(X', X)(K(X, X) + \sigma^2_{e1} I_f)^{-1} Y_1}$ of the GP1 model $\boldsymbol{y_1(X')}|\,(\boldsymbol{X}, \boldsymbol{Y_1})$.

2: **Compute** the first-order index $\boldsymbol{S2_i}$ and closed-order index $\boldsymbol{S2^C_{\psi_i}}$ through performing the GSA computations as Eq.(7-10) on the the mean prediction $\boldsymbol{\mu_{2*}(X') = K(X', X)(K(X, X) + \sigma^2_{e2} I_f)^{-1} Y_2}$ of the GP2 model $\boldsymbol{y_2(X')}|\,(\boldsymbol{X}, \boldsymbol{Y_2})$.

3: **Compute** the first-order index $\boldsymbol{S3_i}$ and closed-order index $\boldsymbol{S3^C_{\psi_i}}$ through performing the GSA computations as Eq.(7-10) on the the mean prediction $\boldsymbol{\mu_{3*}(X') = K(X', X)(K(X, X) + \sigma^2_{e3} I_f)^{-1} Y_3}$ of the GP3 model $\boldsymbol{y_3(X')}|\,(\boldsymbol{X}, \boldsymbol{Y_3})$,

4: **Extract** the important input group $\boldsymbol{\psi^*}$ from the first-order indices $\boldsymbol{S1_i, S2_i, S3_i}$ and closed-order indices $\boldsymbol{S1^C_{\psi_i}, S2^C_{\psi_i}, S3^C_{\psi_i}}$

5: **return** The important input group $\boldsymbol{\psi^*}$ for all three GP models with the corresponding data sets

We implemented the multiple GP models based global sensitivity analysis using the three GP models for the IVT processes. The first-order indices s $\boldsymbol{S1_i, S2_i, S3_i}$ and closed-order indices $\boldsymbol{S1^C_{\psi_i}, S2^C_{\psi_i}, S3^C_{\psi_i}}$ are presented in Figure 5 and 6. Figure 5 demonstrates that NTPs and Mg are the dominant factors across all three models with the corresponding datasets, as their first-order indices are significantly higher than those of the other three factors. Once exception is the concentration of the DNA template, which shows high importance in the GP2 model with data replicate, but plays a much smaller role in the computations for the other two GP models.

Meanwhile, Figure 6 shows that the cumulative indices for NTPs and Mg account for more than half of the importance in the RNA yield output across all three GP models and datasets. This confirms that the concentrations of NTPs, Mg and their interactions form the most important input group $\boldsymbol{\psi^*}$ for all three GP models. The importance of these reagents may provide

valuable insights for optimizing material cost in RNA manufacturing, where high mRNA yield is critial. For instance, further optimizing the composition of Mg and NTPs to enhance yield, along with improving NTP utilization for cost reduction, could be a feasible approach. An efficient model based cost optimization framework could be developed to achieve goals effectively.

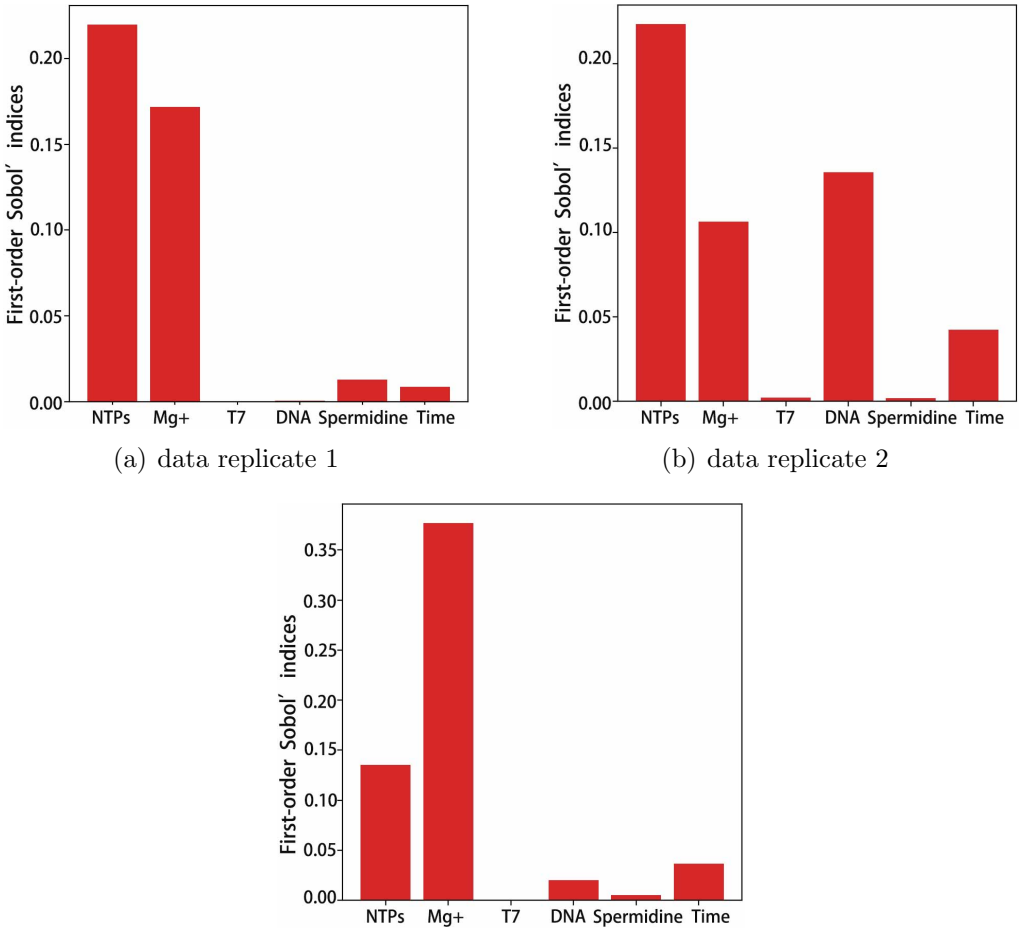

(a) data replicate 1

(b) data replicate 2

(c) the average data of two replicates

Figure 5: First-order indices for mRNA yields from the three models with the corresponding data sets (a) GP1 model from data replicate 1 (b) GP2 model from data replicate 2 (c) GP3 model from the average data

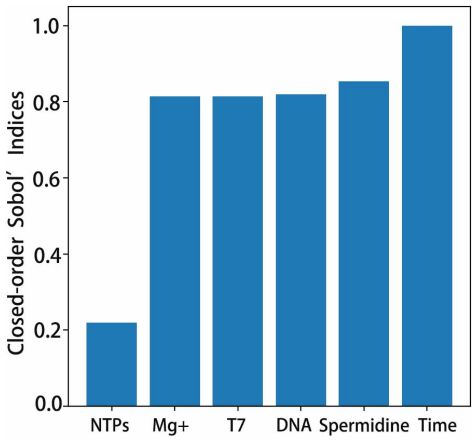

(a) data replicate 1

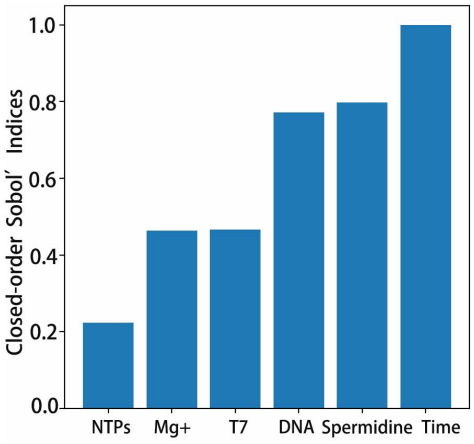

(b) data replicate 2

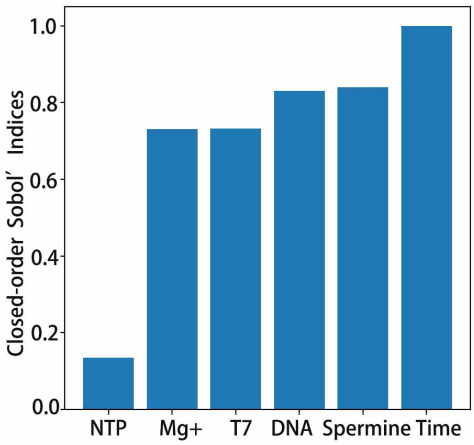

(c) the average data of two replicates

Figure 6: Closed-order indices for mRNA yields from the three models with the corresponding data sets (a) GP1 model from data replicate 1 (b) GP2 model from data replicate 2 (c) GP3 model from the average data

5. Multiple GP models based optimization for IVT processes

The previous multiple GP models based GSA calculations identified key reagents affecting mRNA yield, providing a potential design space for optimization in traditional computations. However, the computational results in this study are approximate due to the limitations of available data and the significant nosie within the data. Relying solely on the computed design

space for optimization may lead to sub-optimal or undesirable outcomes. Additionally, the off-line computation is not extremely resource-intensive, allowing flexibility in approach.

5.1. Multiple GP models based efficient optimization

To determine the optimal operating conditions for maximizing mRNA yield, an efficient optimization scheme was proposed using the three developed GP models, which demonstrated relatively high accuracy. A three-GP model-based iterative procedure was introduced to compute the optimal operating conditions for high mRNA yield across all three models.

Since the GP3 model incorporates data from both replicates, it is expected to have fewer predictive errors compared to GP1 and GP2. As a result, the GP3 model was used as the benchmark surrogate for multi-start optimization to identify operating conditions that yield desirable mRNA outputs. However, because the GP3 model relies on averaged data, it may not fully capture the complexities of process variability and experimental errors, which could be overlooked by a single predictive model. Therefore, it is essential to incorporate the original data from both replicates.

In this approach, the two other GP models (GP1 and GP2), corresponding to the individual replicates, were used as constraints to verify whether the high mRNA yield conditions generated by the GP3 model would also satisfy the predictions of the other two models. This reformulates the problem as a constrained optimization problem. Since the objective function and constraints involve non-convex GP models, we introduced multiple starting points for the local optimization solver (in this case, the Broyden-Fletcher-Goldfarb-Shanno (BFGS) algorithm in Scipy). To further explore the computational impact of constraints, we first solved the relaxed unconstrained optimization problem and then checked the constraints afterward.

It is important to note that , this approach assumes that combining the three GP models, base on a relatively large number of initial samples, can roughly capture the global behavior of the complex IVT system. If this assumption proves invalid, a sequential Bayesian optimization procedure would be employed, iteratively generating new samples to update the GP models and reduce predictive uncertainty until they are sufficiently accurate. The details multiple GP models based optimization algorithm for IVT processes is outlined below.

Algorithm 3 Multiple GP models based optimization algorithm for IVT processes

Inputs: $\boldsymbol{\Omega}$: design space range;
N_1: number of multi-start points for optimization (N_1=100);
$\boldsymbol{N_2}$: number of samples for experimental validations (N_2=3)
$\boldsymbol{(X, Y_1)}$: data set from experiment replicate 1;
$\boldsymbol{(X, Y_2)}$: data set from experiment replicate 2;
$\boldsymbol{(X, Y_3)}$: data set of the averaged data;
$\boldsymbol{Y_b}$: threshold for high mRNA yield (in this work , $\boldsymbol{Y_b}$ = 10 (g/L));
GP1 model from replicate 1: $\boldsymbol{y_1(X')|\,(X, Y_1)}$;
GP2 model from replicate 2: $\boldsymbol{y_2(X')|\,(X, Y_2)}$;
GP3 model from the averaged data: $\boldsymbol{y_3(X')|\,(X, Y_3)}$.

Outputs: $\boldsymbol{X'_*}$: Operating conditions for high mRNA yield $\boldsymbol{Y(X'_*)}$

$\boldsymbol{N_h = 0}$
while $\boldsymbol{N_h < N_2}$ **do**
  Generate N_1 Latin hypercube samples $\boldsymbol{X^{N_1}}$ within the design space $\boldsymbol{\Omega}$
  Compute the optimal solutions set $\boldsymbol{(X_{N_1}, Y_{N_1})}$ through multi-start optimization with the multiple (N_1) initialisation samples $\boldsymbol{X^{N_1}}$:

$$\begin{aligned} \min_{\mathbf{X'}} \quad & \mathbf{Y_{N_1}} = \boldsymbol{\mu}_{3*}(\mathbf{X'}) = \mathbf{K}(\mathbf{X'}, \mathbf{X}) \left(\mathbf{K}(\mathbf{X}, \mathbf{X}) + \sigma_{e3}^2 \mathbf{I_f}\right)^{-1} \mathbf{Y_3} \\ \text{subject to} \quad & \mathbf{X'} \in \boldsymbol{\Omega} \end{aligned} \tag{12}$$

  Select the sub-sample set $\boldsymbol{(X_h, Y_h)}$ from the set $\boldsymbol{(X_{N_1}, Y_{N_1})}$ where:
  $\boldsymbol{\mu_{1*}(X_h) = K(X_h, X)(K(X, X) + \sigma_{e1}^2 I_f)^{-1} Y_1 \geq Y_b}$ and
  $\boldsymbol{\mu_{2*}(X_h) = K(X_h, X)(K(X, X) + \sigma_{e2}^2 I_f)^{-1} Y_2 \geq Y_b}$
end while
Sort the sample set $\boldsymbol{(X_h, Y_h)}$ by $\boldsymbol{Y_h}$ in descending order
Select the top N_2 samples:

$$\boldsymbol{(X'_*, Y(X'_*))} = \mathrm{Top}_{N_2}\left(\boldsymbol{(X_h, Y_h)}\right) \tag{13}$$

return Operating conditions $\boldsymbol{X'_*}$ for high mRNA yield $\boldsymbol{Y(X'_*)}$

The above Algorithm 3 was implemented to determine the computational operating conditions of high mRNA yield. Firstly, a multi-start optimisation procedure was applied to the multiple GP models, generating three ($\boldsymbol{N_2}$) operating conditions that satisfied all three surrogate GP models for high mRNA yield. Subsequently, three experimental replicates were performed for each of the three selected optimal conditions to validate the identified "optimum" samples.

Table 3 provides a comparison between predicted yields (from the proposed multiple GPs) and actual experimental yields along with the NTP utilization. The differences between the predictive optimums and experimental values are relatively small for both mean values and variances, demonstrating the efficiency of the multiple GP models based multi-start optimization framework.

Specifically, two of the experimental yields are high with mean values exceeding the set threshold of $\boldsymbol{Y_b}$=10 g/L in the computational framework, and one experimental result (9.5 g/L) is very close to the threshold. This suggests that the initial computational goal has been nearly achieved. Additionally, the RNA yield is improved from the previous 11.9 g/L to 12.4 g/L. While this improvement is modest, it is likely due to the already high baseline established by the initial experimental design. Nonetheless, the proposed computational approach offers efficient strategies to identify the different operating conditions for high RNA yield while minimizing experimental costs. Moreover, the discrepancies between the experimental and GP predicted mean values are less than 30%, which is acceptable given the significant fluctuations typically seen in bio-process data. In terms of yield variance, the predictive values are under 1g/L, while the experimental variances are slightly higher. For the third computational computational "optimum" condition, the variance values are small and closely aligned between predictions and experimental results, likely due to the high stability of this operating condition. Additionally, extra experimental data show that NTP utilization under the three generated conditions is high, indicating minimal material waste. Thus, the computed optimal conditions are beneficial for achieving high yields and reducing costs, and they may be suitable for large-scale manufacturing applications.

For comparison, the results from a single GP model based optimization algorithm (showed as algorithm 3) are also provided. The key difference between the two methodologies is whether the separate GP model are included to validate the computed "optimum" conditions from the benchmark GP

model. Table 4 provides a comparison between predicted yields (from the single GP) and actual experimental yields along with the NTP utilization. The differences between the predictive optimums and experimental values are relatively small for two of three conditions (less than 10% for the errors of predicted mean values) with high experimental values (more than 11.0 g/L). However, the remaining one includes much higher error (greater than 40%) with medium practical mRNA yield (around 7.5 g/L). The test results on the two GP under this condition shows lower mRNA yield (less than 6 g/L), which can be filtered through our proposed multiple GP based optimization framework. This demonstrates the advantages of the multiple GP optimization framework over single GP one, avoiding potential conditions for low mRNA yields.

Table 3: Comparison between the predictive (Multiple GP models based optimization) and practical experiment yields along with the NTP utilization under the generated operation conditions

Number	Predictive (GP3) Yield(g/L)	Experiment Yield (g/L)	Errors (mean value)	NTP utilization	GP1 Yield(g/L)	GP2 Yield(g/L)
1	13.2 ± 0.7	11.4±1.6	15.7%	80%	13.0± 1.1	12.9± 0.5
2	12.0 ± 0.7	9.5± 1.9	26.3%	70%	13.0± 1.3	12.1± 0.4
3	13.1 ±0.6	12.4± 0.5	5.6%	86%	12.3± 0.7	11.0± 0.4

Algorithm 4 Single GP based optimisation algorithm for IVT processes

Inputs: $\boldsymbol{\Omega}$: design space range;

N_1: number of multi-start points for optimization (N_1=100);

$\boldsymbol{N_2}$: number of samples for experimental validations (N_2=3)

$\boldsymbol{(X, Y_1)}$: data set from experiment replicate 1;

$\boldsymbol{(X, Y_2)}$: data set from experiment replicate 2;

$\boldsymbol{(X, Y_3)}$: data set of the averaged data;

Build GP3 model from the averaged data: $\boldsymbol{y_3(X')|\,(X, Y_3)}$.

Outputs: $\boldsymbol{X'_*}$: Operating conditions for high mRNA yield $\boldsymbol{Y(X'_*)}$

1: $\boldsymbol{N_h = 0}$

2: **while** $\boldsymbol{N_h < N_2}$ **do**

3: **Generate** N_1 Latin hypercube samples $\boldsymbol{X^{N_1}}$ within the design space $\boldsymbol{\Omega}$

4: **Compute** the optimal solutions set $\boldsymbol{(X_{N_1}, Y_{N_1})}$ through multi-start optimization with the multiple (N_1) initialisation samples $\boldsymbol{X^{N_1}}$:

$$\begin{aligned} \min_{\mathbf{X'}} \quad & \mathbf{Y_{N_1}} = \boldsymbol{\mu}_{3*}(\mathbf{X'}) = \mathbf{K}(\mathbf{X'}, \mathbf{X}) \left(\mathbf{K}(\mathbf{X}, \mathbf{X}) + \sigma_{e3}^2 \mathbf{I_f}\right)^{-1} \mathbf{Y_3} \\ \text{subject to} \quad & \mathbf{X'} \in \boldsymbol{\Omega} \end{aligned} \tag{14}$$

5: **end while**

6: **Sort** the sample set $\boldsymbol{(X_h, Y_h)}$ by $\boldsymbol{Y_h}$ in descending order

7: **Select** the top N_2 samples:

$$\boldsymbol{(X'_*, Y(X'_*))} = \mathrm{Top}_{N_2}\left(\boldsymbol{(X_h, Y_h)}\right) \tag{15}$$

8: **return** Operation conditions $\boldsymbol{X'_*}$ for high mRNA yield $\boldsymbol{Y(X'_*)}$

Table 4: Comparison between the predictive (Single-GP model based optimizations) and practical experiment yields under the generated operation conditions

Number	Predictive (GP3) Yield(g/L)	Experiment Yield (g/L)	Errors (mean value)	GP1 Yield(g/L)	GP2 Yield(g/L)
1	10.7± 0.5	7.5 ± 0.4	42.7%	4.7± 0.9	5.4± 0.7
2	11.3 ± 0.4	12.3 ± 0.8	8.1%	12.6± 1.2	13.4± 0.6
3	12.8 ±0.6	11.8 ±0.7	8.5%	13.0± 0.8	11.8± 0.6

6. Conclusion

This paper proposes a global sensitivity analysis and efficient optimization framework for IVT processes based on multiple Gaussian process models. Specifically, multiple GP models were constructed using data replicates from practical experiments. Global sensitivity analysis was then applied to these models, successfully identifying the key factor group influencing mRNA yield in IVT processes. In addition, the combination of multiple GP models and efficient optimization procedures was implemented to determine optimal operating conditions for high mRNA yield, which were validated by experimental data.

However there are some limitations. The multiple GP models were built on a limited number of data sets and replicates, leading to potential uncertainty in the computational results. Given that mRNA technology developed in this work provide valuable insights for process development and optimization at this early stage.

In the future, further experiments will be needed to gain a more accurate understanding of this complex process. Additionally, the proposed framework will be refined and applied to more complex computations, incorporating critical quality attributes of RNA products and additional key performance indicators of the manufacturing process.

T

CRediT authorship contribution statement

Min Tao: Writing – review and editing, Writing – original draft, Visualization, Validation, Software, Resources, Methodology, Investigation, Formal analysis, Data curation, Conceptualization. **Adithya Nair**: Review and editing, Validation, Formal analysis, Data curation. **Ioanna Kalospyrou**: Review and editing. **Robert A Milton**: Software. **Mabrouka Maamra**: Project administration. **Zoltan Kis**: Review and editing, Supervision, Resources, Project administration, Funding acquisition, Formal analysis, Conceptualization. **Joan Cordiner**: Review and editing, Supervision, Resources, Project administration, Funding acquisition, Formal analysis, Conceptualization. **Solomon F Brown**: Review and editing, Supervision, Resources, Project administration, Funding acquisition, Formal analysis, Conceptualization.

Acknowledgements

This work is supported by Wellcome Leap as part of the R3 Program. Thanks for the helps from other team members Dr. Kate A Loveday, Dr. Ehsan Nourafkan, Mr. Mahdi Ahmed, Mr. Joseph Middleton Dr. Emma N Welbourne, and Prof. Mark J Dickman.

References

[1] J. Bedford, J. Farrar, C. Ihekweazu, G. Kang, M. Koopmans, J. Nkengasong, A new twenty-first century science for effective epidemic response, Nature 575 (2019) 130–136.

[2] S. Jain, A. Venkataraman, M. E. Wechsler, N. A. Peppas, Messenger rna-based vaccines: Past, present, and future directions in the context of the covid-19 pandemic, Advanced drug delivery reviews 179 (2021) 114000.

[3] mRNA-based vaccines, therapeutics: an in-depth survey of current, upcoming clinical applications, Wang, yu-shiuan and kumari, monika and chen, guan-hong and hong, ming-hsiang and pei-yi yuan, joyce and tsai, jui-ling and wu, han-chung, Journal of Biomedical Science 30 (2023) 84.

[4] N. Pardi, M. J. Hogan, F. W. Porter, D. Weissman, mrna vaccines - a new era in vaccinology, Nature Reviews / Drug Discovery 17 (2018) 261–279.

[5] A.-K. Minnaert, H. Vanluchene, R. Verbeke, I. Lentacker, S. C. De Smedt, K. Raemdonck, N. N. Sanders, K. Remaut, Strategies for controlling the innate immune activity of conventional and self-amplifying mrna therapeutics: Getting the message across, Advanced drug delivery reviews 176 (2021) 113900.

[6] A. B. van Asbeck, A. Perdrix, A. Willis, C. Martin, D. Lee, E. Smith, H. Makatsoris, J. Fraser, J. DeSimone, K. LeShane, et al., Wellcome leap: Unconventional projects. funded at scale., wellcomeleap.org (2021).

[7] S. S. Rosa, D. M. Prazeres, A. M. Azevedo, M. P. Marques, mrna vaccine manufacturing: Challenges and bottlenecks, Vaccine 39 (2021) 2190–2197.

[8] G. Maruggi, C. Zhang, J. Li, J. B. Ulmer, D. Yu, mrna as a transformative technology for vaccine development to control infectious diseases, Molecular Therapy 27 (2019) 757–772.

[9] N. Armbruster, E. Jasny, B. Petsch, Advances in rna vaccines for preventive indications: A case study of a vaccine against rabies, Vaccines 7 (2019) 1–12.

[10] A. Schmidt, H. Helgers, F. L. Vetter, A. Juckers, J. Strube, Digital twin of mrna-based sars-covid-19 vaccine manufacturing towards autonomous operation for improvements in speed, scale, robustness, flexibility and real-time release testing, Processes 9 (2021) 748.

[11] S. Daniel, Z. Kis, C. Kontoravdi, N. Shah, Quality by design for enabling rna platform production processes, Trends in Biotechnology (2022).

[12] D. van de Berg, Z. Kis, C. F. Behmer, K. Samnuan, A. K. Blakney, C. Kontoravdi, R. Shattock, N. Shah, Quality by design modelling to support rapid rna vaccine production against emerging infectious diseases, npj Vaccines 6 (2021) 65.

[13] S. Arnold, M. Siemann, K. Scharnweber, M. Werner, S. Baumann, M. Reuss, Kinetic modeling and simulation of in vitro transcription by phage t7 rna polymerase, Biotechnology and bioengineering 72 (2001) 548–561.

[14] S. Akama, M. Yamamura, T. Kigawa, A multiphysics model of in vitro transcription coupling enzymatic reaction and precipitation formation, Biophysical journal 102 (2012) 221–230.

[15] R. Braatz, N. M. Stover, K. Ganko, Mechanistic modeling of in vitro transcription, Preprint (2023).

[16] J. N. Kutz, Data-driven modeling & scientific computation: methods for complex systems & big data, OUP Oxford, 2013.

[17] J. S. Young, W. F. Ramirez, R. H. Davis, Modeling and optimization of a batch process for in vitro rna production, Biotechnology and Bioengineering 56 (1997) 210–220.

[18] M. A. Nielsen, Neural networks and deep learning, volume 25, Determination press San Francisco, CA, USA, 2015.

[19] S. S. Rosa, D. Nunes, L. Antunes, D. M. Prazeres, M. P. Marques, A. M. Azevedo, Maximizing mrna vaccine production with bayesian optimization, Biotechnology and Bioengineering 119 (2022) 3127–3139.

[20] M. Von Stosch, R. Oliveira, J. Peres, S. F. de Azevedo, Hybrid semi-parametric modeling in process systems engineering: Past, present and future, Computers & Chemical Engineering 60 (2014) 86–101.

[21] G. Bonner, E. Lafer, R. Sousa, The thumb subdomain of t7 rna polymerase functions to stabilize the ternary complex during processive transcription, Journal of Biological Chemistry 269 (1994) 25129–25136.

[22] C.-S. Cheng, Theory of factorial design: Single-and multi-stratum experiments, CRC Press, 2013.

[23] W.-L. Loh, On latin hypercube sampling, The annals of statistics 24 (1996) 2058–2080.

[24] S. Theodoridis, Machine learning: a Bayesian and optimization perspective, Academic press, 2015.

[25] C. K. Williams, C. E. Rasmussen, Gaussian processes for machine learning, volume 2, MIT press Cambridge, MA, 2006.

[26] A. S. Yeardley, S. Bellinghausen, R. A. Milton, J. D. Litster, S. F. Brown, Efficient global sensitivity-based model calibration of a high-shear wet granulation process, Chemical Engineering Science 238 (2021) 116569.

[27] A. Saltelli, M. Ratto, T. Andres, F. Campolongo, J. Cariboni, D. Gatelli, M. Saisana, S. Tarantola, Global sensitivity analysis: the primer john wiley & sons; 2008, 2008.

[28] R. Milton, S. Brown, Romcomma, URL: https://github.com/COMMA/rom-comma (2019).

[29] S. Razavi, A. Jakeman, A. Saltelli, C. Prieur, B. Iooss, E. Borgonovo, E. Plischke, S. L. Piano, T. Iwanaga, W. Becker, et al., The future

of sensitivity analysis: An essential discipline for systems modeling and policy support, Environmental Modelling & Software 137 (2021) 104954.

[30] M. Tao, J. O. Ejeh, R. A. Milton, J. Cordiner, S. F. Brown, Multiple-output gaussian process based global sensitivity analysis for the cost-performance of electric vehicle in the united kingdom, in: Computer Aided Chemical Engineering, volume 52, Elsevier, 2023, pp. 1433–1438.